JOURNAL OF MATERIALS SCIENCE 21 (1986) 346–354

A hydriding kinetic model of the Mg_2Ni–H_2 system

M. Y. SONG, M. PEZAT, B. DARRIET, J. Y. LEE*, P. HAGENMULLER
*Laboratoire de Chimie du Solide du CNRS, 351 cours de la Libération, 33405 Talence Cedex, France and *Department of Materials Science and Engineering, Korea Advanced Institute of Science and Technology, PO Box 150, Chongryang, Seoul, Korea*

The hydriding kinetics of an Mg_2Ni alloy are investigated under hydrogen pressures from 2.5 to 8 bar (0.25 to 0.8 MPa) at various temperatures ($543 \leqslant T \leqslant 583$ K). The hydriding reaction of Mg_2Ni progresses by a nucleation and growth mechanism. The rate-controlling step is analysed to be the forced flow of hydrogen molecules through pores, interparticle channels or cracks of the sample, involving heat-transfer control.

1. Introduction

Investigation of hydriding kinetics can lead to an understanding of the hydriding reaction mechanisms, but very few studies have been reported [1–4]. In this paper a model of the hydriding kinetics of Mg_2Ni will be proposed and theoretical rate equations established by considering the morphology and the surface state of the hydrided sample. The application of this model to hydriding kinetic data will enable us to determine the rate controlling steps.

2. Experimental details

The hydrogen was supplied by l'Air Liquide (U quality) and was purified by passing through a column filled with magnesium chips maintained at 823 K. To prepare the Mg_2Ni alloy, we used magnesium powder (Ventron GmbH, West Germany, −50 mesh, 99.8% purity) and nickel (Cerac Inc, USA, −325 mesh, 99.9% purity). A mixture of magnesium and nickel in the proportions corresponding to the composition $Mg_{2.05}Ni$ was pressed under 3 ton cm^{-2} (290 MPa) for 2 min in a vacuum. This composition was chosen as during the reaction a small quantity of magnesium is evaporated. The pellet was then melted under an argon atmosphere of 3 bar (0.3 MPa) at 1173 K for 1 h in a molybdenum crucible. After grinding and pressing under argon, it was annealed at 973 K for 60 h under an argon atmosphere.

Magnetic measurements showed that the sample exhibited paramagnetic behaviour, and very small amounts of $MgNi_2$ and MgO as impurities were detected from the X-ray diffraction patterns. A micrograph by back-scattering electrons revealed some inclusions of a nickel-rich phase (probably $MgNi_2$) in the Mg_2Ni matrix.

The amount of Mg_2Ni used was about 0.90 g. The particle size of the starting material was smaller than 63 μm. The apparatus for hydriding was previously described elsewhere [5]. The hydrogen pressures in the reactor were maintained nearly constant during the reaction by employing appropriate dosing hydrogen from a known volume. The pressure drop in the reactor was 1 to 8% of the chosen pressure in the course of our measurements. The pressure variation of hydrogen in the known volume (due to dosing hydrogen) permits the calculation of the quantity of hydrogen absorbed by the sample as a function of time. A thermocouple was located within the bottom wall of the reactor. Changes in temperatures were recorded during the reaction.

The activation of the sample is considered to be achieved at 7 bar (0.7 MPa) hydrogen pressure at 573 K after 13 cycles. The hydrogen absorption rates by the activated Mg_2Ni are measured at hydrogen pressures from 2.5 to 8 bar (0.25 to 0.8 MPa), at five different temperatures between 543 and 583 K.

3. Results

We define the fraction F which has reacted during t min as follows: $F \equiv$ number of H_2 moles absorbed during t min divided by number of H_2 moles calculated on the assumption that 100% of the activated sample is hydrided to the composition Mg_2NiH_4.

Fig. 1 shows a representative plot of the influence of hydrogen pressures P_0 on the hydrogen absorption by the activated Mg_2Ni at 563 K.

Fig. 2 shows a representative plot of the influence of temperature T at a constant hydrogen pressure of 5.5 bar (0.55 MPa).

Fig. 3 shows the initial parts of the reacted fraction (F) against time (t) curves at 543 K, scaled up. At the very beginning they exhibit an extremely rapid hydrogen absorption up to $F \simeq 0.045$. Those obtained at 2.5, 3 and 3.5 bar (0.25, 0.3 and 0.35 MPa) show incubation periods of about 10, 1 and 0.5 min respectively. The initial point S (as indicated on Fig. 3) is reached as soon as hydrogen is charged in the reactor. The times (about 0.25 min) for the points are the periods required for dosing the hydrogen in order to maintain the chosen pressure. It is considered that the region from $F = 0$ to the point S corresponds to a non-saturated solid solution (Region α in Fig. 3).

0022–2461/86 $03.00 + .12

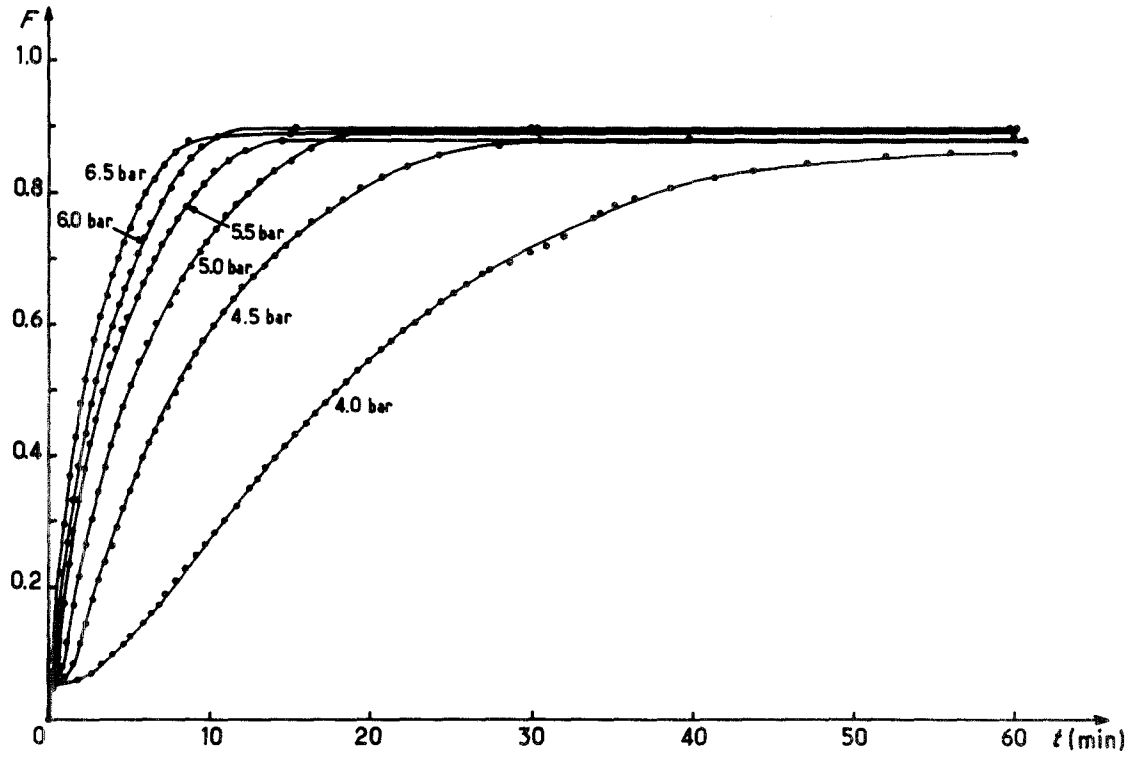

Figure 1 Influence of hydrogen pressure P_0 on hydrogen absorption by activated Mg_2Ni at 563 K. 1 bar = 0.1 MPa.

After this initial period, the actual hydriding reaction begins (Region β in Fig. 3). Our main interest is devoted to Region β.

4. Models of hydriding kinetics in the Mg_2Ni–H_2 system

The microstructure of the Mg_2Ni sample, activated under various experimental conditions, was observed by transmission electron microscopy and by scanning electron microscopy (SEM) (Fig. 4). The particles have irregular shapes, variable size distribution and are porous.

Thus it is not reasonable to derive rate equations on the assumption that they have uniform sizes and regular shapes as if they were spheres or cylinders, etc. In addition, the phase transformation of Mg_2Ni from α-solid solution into the hydride phase involves a volume expansion of about 24% [6].

For these reasons, it is impossible to establish a simple relation between the variation of the reaction-interfacial area and the reacted fraction F. As a consequence the rate equations for the hydriding of the activated Mg_2Ni cannot be given as a simple function of F. Rate equations are developed to analyse the

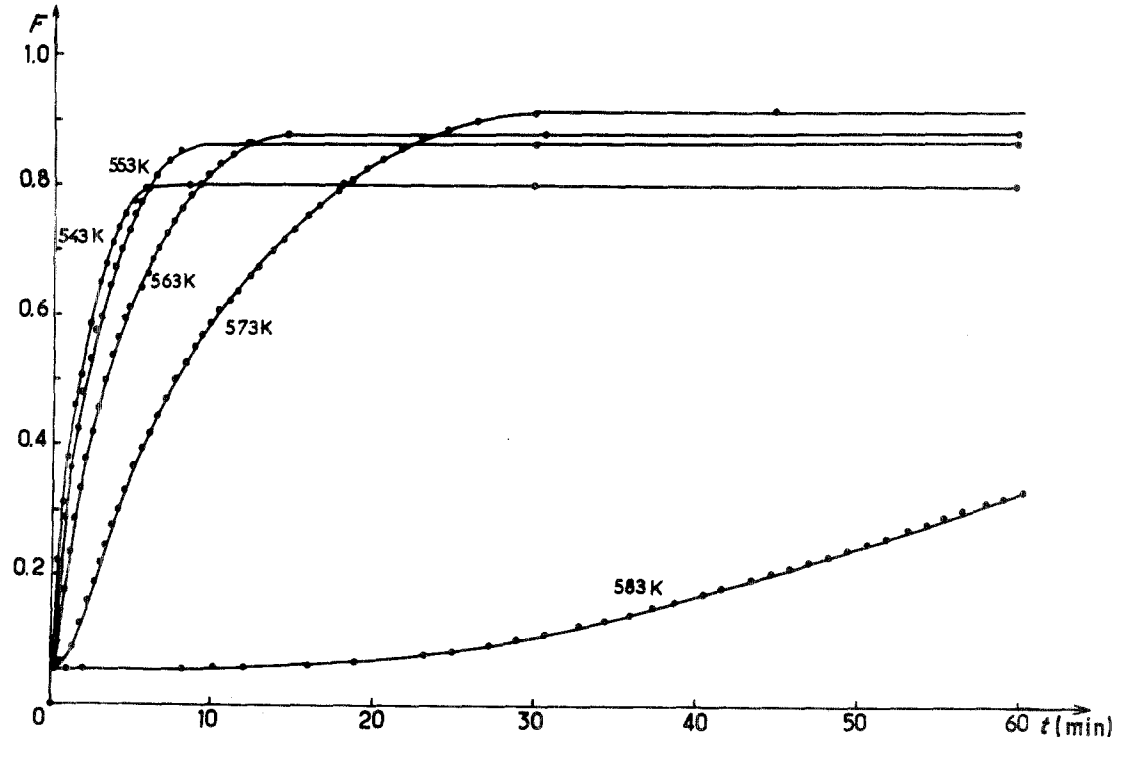

Figure 2 Influence of temperature T on hydrogen absorption by activated Mg_2Ni under 5.5 bar H_2 (0.55 MPa).

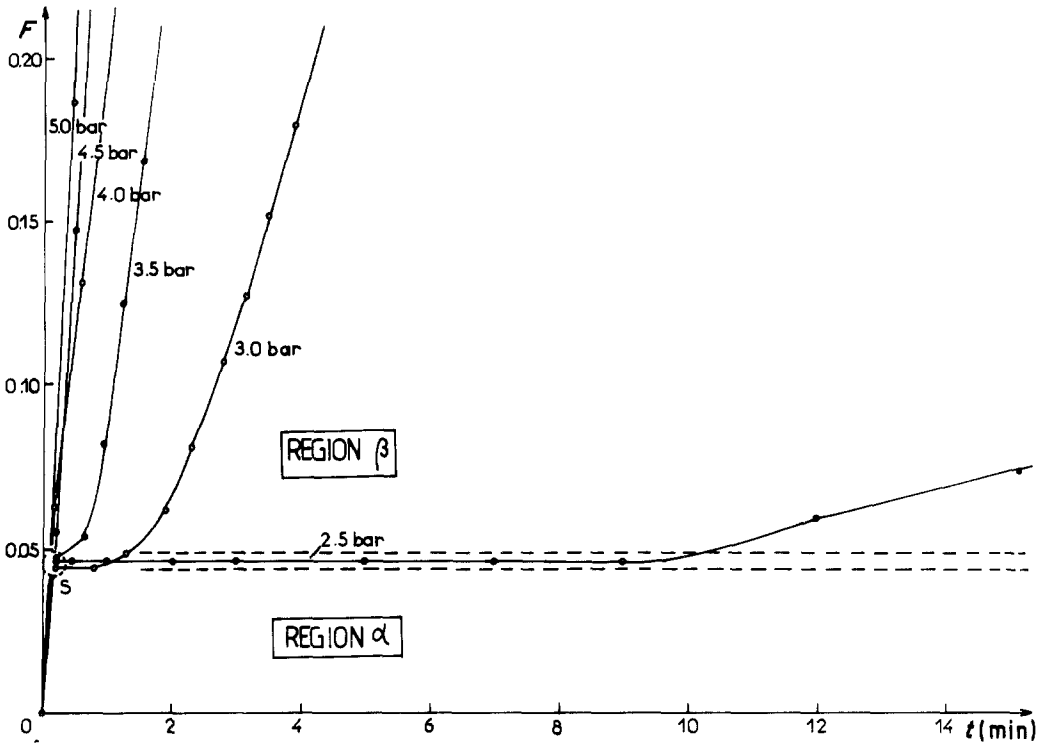

Figure 3 Initial parts of the reacted fraction (F) against time (t) curves at 543 K. 1 bar = 0.1 MPa.

hydriding kinetics for a relatively small range of the reacted fraction. So as to conserve a nearly equal reaction-interfacial area, the influences of hydrogen pressure and temperature on the hydriding rates have been studied in the same ranges of the reacted fraction.

4.1. The hydriding process of activated Mg_2Ni

The activated Mg_2Ni shows a slight ferromagnetic behaviour indicating nickel segregation [7]. Seiler *et al.* [8] have shown by X-ray photoemission spectroscopy and Auger electron spectroscopy that some metallic nickel segregated to the surface of Mg_2Ni exposed to 1 to 100 L O_2 (where 1 L = 10^{-6} torr sec). This results from the selective oxidation of magnesium by oxygen [7]. The segregated nickel can act as active sites for the dissociative chemisorption of hydrogen [9].

The hydriding process of activated Mg_2Ni can be described under three headings: (a) Gas-phase mass flow, i.e. mass transport of H_2 molecules up to the surface of Mg_2Ni of nickel; (b) intrinsic processes as follows:

(i) dissociative chemisorption of H_2 molecules on the surface of Mg_2Ni or nickel;

(ii) for hydrogen atoms chemisorbed on the surface of nickel, surface diffusion of hydrogen atoms on the nickel surface either to the surface of Mg_2Ni or to the

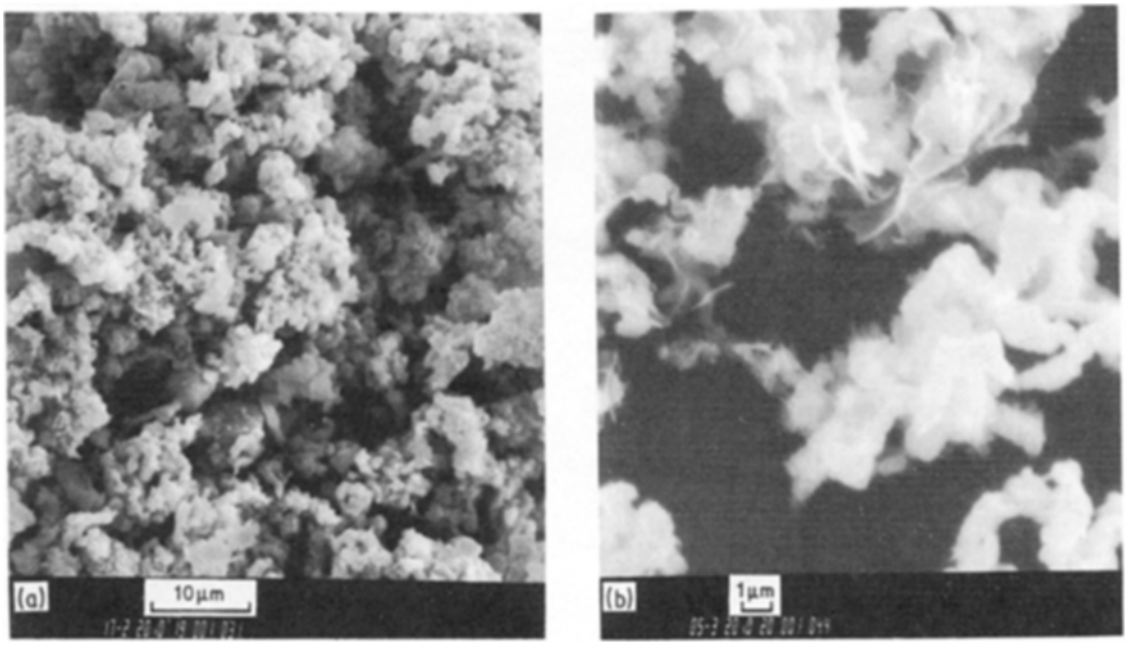

Figure 4 Microstructure of Mg_2Ni by SEM: (a) after 25 hydrogen absorption–desorption cycles (× 1300), (b) after 39 cycles (× 4150).

grain boundary of nickel and magnesium oxide, and also diffusion of hydrogen atoms through the grain boundaries between nickel and magnesium oxide;

(iii) transition of hydrogen atoms from their chemisorbed state into their absorbed state;

(iv) diffusion of hydrogen atoms through the growing layer of hydride;

(v) phase transformation (α-solid solution of hydrogen in $Mg_2Ni \rightarrow$ hydride);

and finally (c) heat flow.

Heat transfer may also be an important step for hydriding. The increase in temperature during the reaction decreases the hydrogen absorption rates by raising the equilibrium plateau pressure (P_{eq}) and causing a diminution of the difference between hydrogen pressure P_0 and P_{eq}, which is related to the hydriding driving force.

4.2. Theoretical rate equations

4.2.1. A model based on a continuous moving boundary

Theoretical rate equations for each step are derived on the assumption that *each step maintains a quasi-steady state at constant temperature and pressure.*

4.2.1.1. Gas-phase mass flow. When the mean free path of the gas molecules (λ) exceeds appreciably the diameter ($2r$) of the pores, or of the interparticle channels or of the cracks (i.e. if $\lambda \gg 2r$), Knudsen flow is the mode of molecular transport. The flow rate R_K is given by

$$R_K = \frac{4}{3} r^3 \left(\frac{2\pi}{RM}\right)^{\frac{1}{2}} T^{-\frac{1}{2}} \frac{(P_0 - P_{eq})}{\Delta L} \quad (1)$$

where R is the gas constant, M the molecular weight of the gas and $(P_0 - P_{eq})/\Delta L$ the gradient of the pressure along the paths (P_0 = hydrogen pressure, P_{eq} = equilibrium plateau pressure), whose shapes are assumed to be cylindrical.

If λ is smaller than $2r$ (i.e. if $\lambda < 2r$), and when a pressure difference is maintained across the pores, channels or cracks, a forced flow occurs. Its rate R_F is given by

$$R_F = \frac{\pi r^4}{8RT\eta} \bar{P} \frac{(P_0 - P_{eq})}{\Delta L} \quad (2)$$

$$= \frac{\pi r^4}{16R\eta} T^{-1}(P_0 + P_{eq}) \frac{(P_0 - P_{eq})}{\Delta L}$$

where η is the viscosity of the gas and $\bar{P}$ the average pressure [10, 11]. At pressures below about 10 bar the viscosity of a gas is independent of pressure and the variation of viscosities of hydrogen is within 5% in the temperature range $543\,K \leqslant T \leqslant 583\,K$ considered in this work. Thus η of Equation 2 can be considered as a constant.

4.2.1.2. Intrinsic processes.

4.2.1.2.1. The dissociative chemisorption of H_2 molecules on the surface of Mg_2Ni or nickel. This step can be expressed as follows [11, 12–14]:

$$H_2 + -\underset{|}{S}-\underset{|}{S}- \underset{k_d}{\overset{k_a}{\rightleftharpoons}} \underset{|}{\overset{H}{S}}-\underset{|}{\overset{H}{S}}- \quad (3)$$

where $-\underset{|}{S}-$ is a surface active site of Mg_2Ni or nickel, and k_a and k_d the rate constants for adsorption and desorption respectively.

If $\theta^{\circ}_{P_{eq}}$ is the equilibrium coverage of surface sites by hydrogen under the equilibrium plateau pressure (P_{eq}) at a given temperature, the chemisorption rate v when the hydrogen pressure is P_0 is given [12, 15] by

$$v = k_a(1 - \theta^{\circ}_{P_{eq}})^2 P_0 - k_d(\theta^{\circ}_{P_{eq}})^2 \quad (4)$$

Let θ°_P be the equilibrium coverage under a hydrogen pressure P. It is then given by

$$\theta^{\circ}_P = \frac{(bP)^{\frac{1}{2}}}{1 + (bP)^{\frac{1}{2}}} \quad (5)$$

where $b = k_a/k_d$. Equation 5 is the form of the Langmuir adsorption isotherm for diatomic molecules.

In the hydriding reaction, when the hydrogen pressure P_0 becomes equal to the equilibrium plateau pressure P_{eq}, the driving force for hydriding is zero, with hydriding rate equal to zero. With this condition Equation 4 can be written as

$$v = k_a(1 - \theta^{\circ}_{P_{eq}})^2(P_0 - P_{eq}) \quad (6)$$

From the kinetic theory of gases, k_a is given by

$$k_a = \delta_a T^{-n} \exp\left(-\frac{E_a}{k_T}\right) \quad (7)$$

where δ_a is a constant, $n = 5/2$ when the adsorbed molecules are localized in the adsorbed state, $n = 1/2$ when the adsorbed molecules are not localized in the adsorbed state, and E_a is the activation energy per mole for adsorption.

The combination of Equations 6 and 7 gives

$$v = \delta_a(1 - \theta^{\circ}_{P_{eq}})^2 T^{-n}(P_0 - P_{eq}) \exp\left(-\frac{E_a}{k_T}\right) \quad (8)$$

where $\delta_a(1 - \theta^{\circ}_{P_{eq}})^2$ is a constant in our experimental conditions [5].

4.2.1.2.2. The surface and grain-boundary diffusion of hydrogen atoms (for hydrogen atoms chemisorbed on the surface of nickel. The surface or grain-boundary diffusion rate R_D can be expressed as follows in the steady state:

$$R_D = -\frac{L_D}{d} D (C_0 - C_{eq}) \quad (9)$$

where L_D is the total length of paths available for hydrogen diffusion on the nickel surfaces or in the grain boundaries, d the average diffusion distance of hydrogen on the nickel surfaces or in the grain boundaries and D the surface or grain boundary diffusivity of hydrogen; C_0 and C_{eq} are given by

$$C_0 = K_0 \theta^{\circ}_{P_0} = \frac{K_0(bP_0)^{\frac{1}{2}}}{1 + (bP_0)^{\frac{1}{2}}} \quad (10)$$

$$C_{eq} = K_0\theta^{\circ}_{P_{eq}} = \frac{K_0(bP_{eq})^{\frac{1}{2}}}{1 + (bP_{eq})^{\frac{1}{2}}} \quad (11)$$

where K_0 is the concentration of single adsorption sites.

4.2.1.2.3. The transition of hydrogen atoms from their chemisorbed state into their absorbed state. The hydrogen absorption rate R_3 is given by

$$R_3 = SK_0k_{f3}(C_0 - C_{eq}) \quad (12)$$

where S is the total surface area of the sample, k_{f3} the forward rate constant of this step, and C_0 and C_{eq} are given by Equations 10 and 11 respectively [11].

4.2.1.2.4. The diffusion of hydrogen atoms through the growing hydride layer. By using the assumption of quasi-steady state, the reacted fraction F at time t is given by

$$F = C[D_H(C_1 - C_2)t]^{\frac{1}{2}} \quad (13)$$

where C is a constant, D_H the diffusivity of hydrogen in the hydride and C_1 and C_2 the concentrations of diffusing hydrogen at the hydrogen–hydride interface and at the hydride–α-solid solution interface respectively. From the concentration of equilibrium of Step 4.2.1.2.3,

$$C_1 = \frac{k_{f3}}{k_{b3}}C_0 = \frac{k_{f3}}{k_{b3}}K_0\theta^{\circ}_{P_0} \quad (14)$$

If $P_0 = P_{eq}$, the hydriding rate is zero. Thus

$$C_2 = \frac{k_{f3}}{k_{b3}}K_0\theta^{\circ}_{P_{eq}} \quad (15)$$

4.2.1.2.5. Phase transformation from an α-solid solution into hydride. For this step the hydrogen absorption rate R_5 is given by

$$R_5 = A_ik_{f5}(C_1 - C_\beta) \quad (16)$$

where A_i is the area of the interface between hydride phase and α-solid solution, k_{f5} the forward rate constant, C_1 the hydrogen concentration at the surface side of the hydride phase ($= (k_{f3}/k_{b3})K_0\theta^{\circ}_{P_0}$) and C_β the hydrogen concentration of the hydride phase ($= (k_{f3}/k_{b3})K_0\theta^{\circ}_{P_{eq}}$).

4.2.2. Nucleation and growth theory

The hydride phase β nucleates in certain regions. The matrix α is then transformed by the advance of the α–β interface out into the matrix α until the regions of β impinge and no α remains.

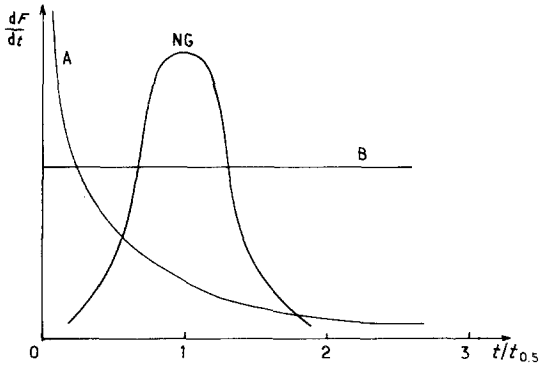

Figure 5 Variation of the hydriding rate dF/dt with reduced time $t/t_{0.5}$. NG = nucleation and growth, A = diffusion of hydrogen atoms through the growing hydride layer, B = all the other steps except heat transfer. For A and B the variation of the reaction-interfacial area is not considered.

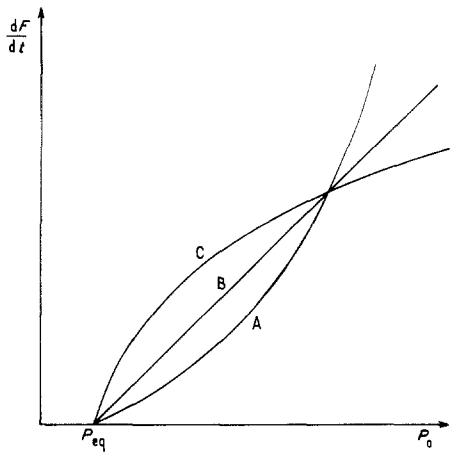

Figure 6 Dependence of the hydriding rate dF/dt on hydrogen pressure P_0 (arbitrary scales) when the rate-controlling step is (A) forced flow, (B) Knudsen flow or dissociative chemisorption of H_2 molecules, (C) all the other steps except heat transfer.

The rate equation for the nucleation and growth is expressed by the Johnson–Mehl–Avrami equation as following [16]:

$$F = 1 - \exp[-N(\dot{g}t)^{\eta}] \quad (17)$$

where F is the growing-phase fraction (i.e. the reacted fraction), N the number of nuclei, $\dot{g}$ the growth rate and η the exponent which is determined by the rate-controlling process, and by growth dimensionality and nucleation rate.

4.3. Variation of hydriding rate dF/dt with time and dependence of hydriding rates on hydrogen pressure P_0 and temperature.

On the basis of the rate equations given above, when each step is rate-controlling, the variation of hydriding rate with time is shown in Fig. 5. The time is expressed in a reduced time scale $t/t_{0.5}$.

The NG curve for the nucleation and growth mechanism shows two distinct trends. The initial one of increasing rates concerns the nucleation and growth stage, the later one the decreasing rates for the stage of growth and impingement among hydride β. In the rate equations for the continuous moving boundary (Section 4.2.1), the variation of the reaction-interfacial area, as the reaction proceeds, is not taken into consideration.

The dependence of hydriding rates on hydrogen pressure and temperature is described by Figs. 6 and 7. In Fig. 6 the curves are drawn in such a way that they intersect at one point.

5. Application of the above models to results of hydriding reactions

5.1. The variation of the hydriding rate dF/dt with time

dF/dt is obtained in various ranges of the reacted fraction F as represented in Fig. 8.

Fig. 9 shows the variation of the hydriding rate dF/dt with time representatively at 563 K under

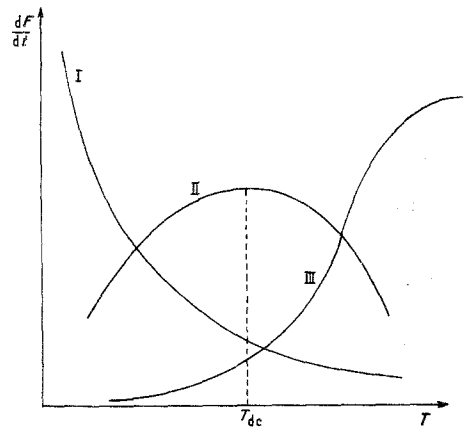

Figure 7 Dependence of the hydriding rate on temperature when the rate-controlling step is (I) mass transport of H_2 molecules (Knudsen flow or forced flow); (II) dissociative chemisorption (localized → $T_{dc} = 2E_a/5R$, not localized → $T_{dc} = 2E_a/R$); (III) all the other steps except heat transfer.

hydrogen pressure 4 to 6.5 bar (0.4 to 0.65 MPa). Its comparison with Fig. 5 clearly shows that the hydriding reaction of Mg_2Ni progresses with the nucleation and growth mechanism under these experimental conditions. Under 6 and 6.5 bar H_2 (0.6 and 0.65 MPa), the initial trend of the nucleation and growth mechanism does not appear. This is considered to be due to the rapid nucleation of the Mg_2Ni hydride under such relatively high pressures, while under lower pressures the slower nucleation of the Mg_2Ni hydride causes an incubation period in the $F-t$ curves and the appearance of the initial trend of the nucleation and growth mechanism.

On the other hand, even though it is impossible to decide the rate-controlling step by simply comparing the result of Fig. 9 with Fig. 5 (as the variation of the reaction surface area is not considered for all the other steps), a comparison of the later part of the $(dF/dt)-t$ curves of Fig. 9 with Fig. 5 suggests that the diffusion of hydrogen atoms through the growing hydride phase may be a rate-controlling step.

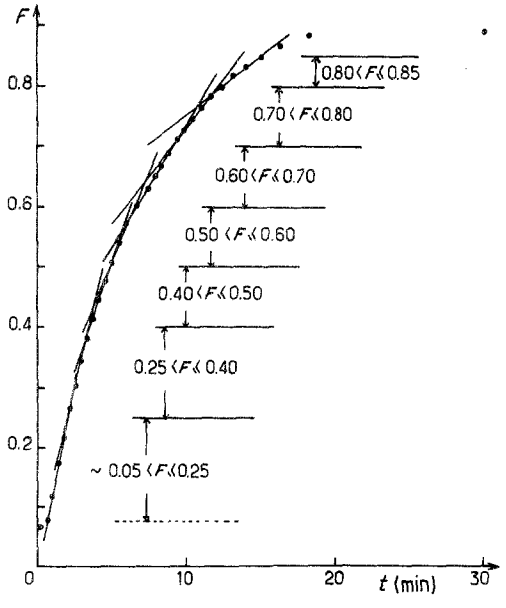

Figure 8 Method used for obtaining the hydriding rate. $T = 563$ K, $P_0 = 5.0$ bar (0.5 MPa).

5.2. Dependence of hydriding rates on hydrogen pressure and temperature

In the above continuously-moving boundary model, the variation of the reaction interface area could not be considered because of the irregular shape and variable size distribution of the activated Mg_2Ni particles. To apply our results to these rate equations, they must be analysed in the same ranges of reacted fractions where the reaction interface areas are equal.

The hydriding rate dF/dt of Mg_2Ni showed relatively good linear dependence on hydrogen pressure in all the different ranges of the reacted fraction.

On the other hand, Fig. 10 shows the variation of the hydriding rate dF/dt of Mg_2Ni against square of hydrogen pressure P_0 at 563 K for the various ranges of reacted fractions. These plots of dF/dt against P_0^2 represent better linearities than those of dF/dt against P_0.

Over extended pressure ranges (at 543 K 2.5 bar (0.25 MPa) $\leqslant P_0 \leqslant$ 6 bar (0.6 MPa), at 583 K 5.5 bar (0.55 MPa) $\leqslant P_0 \leqslant$ 8.5 bar (0.85 MPa)) the hydriding rates showed obviously second-order dependences on hydrogen pressure.

To investigate the dependence on hydriding rates on hydrogen pressure at different temperatures (543 K $\leqslant T \leqslant$ 583 K), hydriding rates have been obtained in the ranges of the reacted fractions $\sim 0.05 < F \leqslant 0.25$ (Fig. 11) and $0.60 < F \leqslant 0.70$ (Fig. 12). These ranges are chosen to represent respectively the initial and the later stage of the hydriding reaction. The data points in the incubation period are not used to determine hydriding rates.

The comparison of this behaviour of the hydriding rates with the theoretical curves of Fig. 6 suggests that the rate-controlling step for the hydriding reaction of Mg_2Ni may be forced flow of H_2 molecules through the pores, the interparticle channels or the cracks.

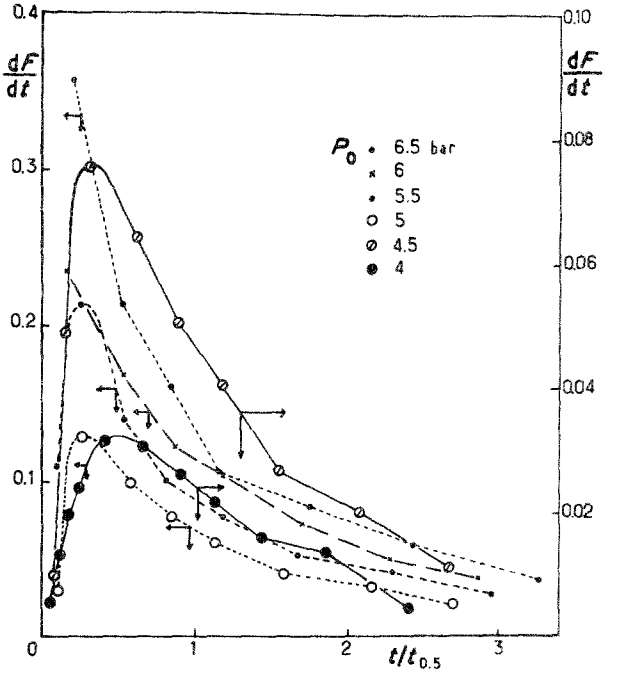

Figure 9 Variation of the hydriding rate dF/dt with reduced time $t/t_{0.5}$ at 563 K.

TABLE I Values of constants at 563 K (P_{eq} = 3.31)

F	($10^3 \times a_2$(min^{-1} bar^{-2}))	b_2 (bar)	$\Delta P_{eq} \equiv b_2 - P_{eq}$ (bar)
$\sim 0.05 < F \leqslant 0.25$	11.95	3.71	0.40
$0.25 < F \leqslant 0.40$	6.89	3.30	−0.01
$0.40 < F \leqslant 0.50$	4.98	3.19	−0.12
$0.50 < F \leqslant 0.60$	2.85	2.42	−0.89
$0.60 < F \leqslant 0.70$	2.66	3.14	−0.17
$0.70 < F \leqslant 0.80$	1.76	2.81	−0.50
$0.80 < F \leqslant 0.85$	1.32	3.31	0

1 bar = 0.1 MPa

The hydriding rate dF/dt can be expressed as a function of hydrogen pressure by

$$\frac{dF}{dt} = a_2(P_0^2 - b_2^2) \quad (18)$$

where a_2 and b_2 are constants which depend on the reacted fraction and the temperature (Tables I and II).

Values of a_2 show inverse temperature dependences in given reacted fractions (Table II). This behaviour of a_2 values agrees well with that of the theoretical curve for the forced-flow control (Fig. 7). In fact, the temperature dependences of a_2 for the forced-flowstep, i.e. a_2 against $1/T$, present very good linearities (Fig. 13).

In other words, the pressure and temperature dependences of hydriding rates, analysed above, clearly show that forced flow is the rate-controlling step in the hydriding process; they eliminate the diffusion of hydrogen atoms through the growing hydride phase from a rate-controlling step, which was suggested as a rate-controlling step from the trends of the later part of dF/dt against t of Fig. 9.

Now we compare the experimental rate equation (Equation 18) with the rate equation for forced-flow control. Equilibrium plateau pressures P_{eq}, the values of b_2 and $\Delta P_{eq}(\equiv b_2 - P_{eq})$ are also given in Tables I and II. Equilibrium plateau pressures P_{eq}, for hydrogen absorption are measured to depend on temperature according to

$$\ln P_{eq}(\text{bar}) = -7.394/T + 14.33 \quad (19)$$

where 1 bar = 0.1 MPa. The ΔP_{eq} values are positive for $\sim 0.05 < F \leqslant 0.25$, while they are less than zero for all the other ranges of the reacted fraction.

Fig. 14 shows the variation of temperature due to the heat of reaction as the hydriding reaction proceeds at 573 K under 7 bar H_2 (0.7 MPa). The temperature increase is about 3.7 K in the beginning of the hydriding reaction and then it decreases; finally the temperature becomes constant. The variation of temperature increase was observed to be more sensitive to hydriding rates than to the experimental temperature.

This variation of temperature causes ΔP_{eq} values to vary like the above trends. The increase in temperature at the beginning leads to a b_2 larger than P_{eq} for a set temperature, giving a positive value of ΔP_{eq}. In the other ranges of the reacted fraction the ΔP_{eq} values become zero or negative as the variation of temperature becomes smaller. This phenomenon suggests that the hydriding reaction of Mg_2Ni is controlled by heat transfer too.

By writing $\Delta P_{eq} \equiv b_2 - P_{eq}$, Equation 18 can be modified to give

$$\frac{dF}{dt} = a_2[P_0^2 - (P_{eq} + \Delta P_{eq})^2] \quad (20)$$

where a_2 and ΔP_{eq} are constants which depend on the reacted fraction and the temperature (Tables I and II).

The temperature dependence of a_2 is expressed from Fig. 13 by the following equations:

$$\sim 0.05 < F \leqslant 0.25$$
$$a_2 = 124.3/T - 0.208 \quad (21)$$

$$0.60 < F \leqslant 0.70$$
$$a_2 = 22.15/T - 0.0367 \quad (22)$$

The value of a_2 diminishes to zero at 598 K in the range of $\sim 0.05 < F \leqslant 0.25$, and at 603 K for $0.60 < F \leqslant 0.70$. This indicates that the hydriding rate will be very small above 603 K in these experimental conditions.

By combining Equations 20 and 21 or 22, we get the following reactions:

$$\sim 0.05 < F \leqslant 0.25 \text{ (initial stage):}$$
$$\frac{dF}{dt} = \left(\frac{124.3}{T} - 0.208\right) \times [P_0^2 - (P_{eq} + \Delta P_{eq})^2] \quad (23)$$

TABLE II Values of constants at various temperatures

T (K)	P_{eq} (bar)	$\sim 0.05 < F \leqslant 0.25$			$0.60 < F \leqslant 0.70$		
		$10^3 \times a_2$ (min^{-1} bar^{-2})	b_2 (bar)	ΔP_{eq} (bar)	$10^3 \times a_2$ (min^{-1} bar^{-2})	b_2 (bar)	ΔP_{eq} (bar)
543	2.04	21.10	2.41	0.37	4.06	2.04	0
553	2.61	17.00	2.89	0.28	3.33	2.50	−0.11
563	3.31	11.95	3.71	0.40	2.66	3.14	−0.17
573	4.16	8.18	4.49	0.33	1.88	3.97	−0.19
583	5.19	5.93	5.45	0.26	1.29	4.76	−0.43

1 bar = 0.1 MPa

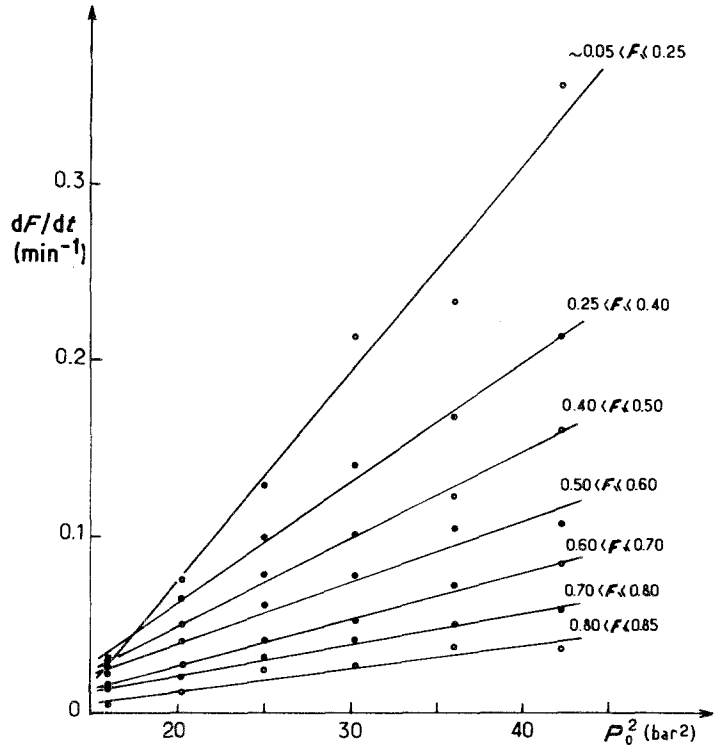

Figure 10 Dependence of the hydriding rate dF/dt on the square of hydrogen pressure P_0 in various ranges of reacted fraction at 563 K.

and

$$0.60 < F \leqslant 0.70 \text{ (later stage):}$$

$$\frac{dF}{dt} = \left(\frac{22.15}{T} - 0.0367\right) \times [P_0^2 - (P_{eq} + \Delta P_{eq})^2] \quad (24)$$

where the values of ΔP_{eq} are given in Table II.

From the above analyses, we can clearly conclude that the hydriding reaction of Mg_2Ni progresses as the nucleation and growth mechanism, and that the rate-controlling step is the forced flow of H_2 molecules through pores, interparticle channels or cracks, involving heat-transfer control.

6. Discussion

The calculation of the heat of formation of the Mg_2Ni hydride gives a value which is about -14.7 kcal mol^{-1} H_2 (-61.6 kJ mol^{-1}) on the basis of Equation 19.

The heat of chemisorption of hydrogen ona nickel surface is reported to be about -30 kcal mol^{-1} H_2 (-125 kJ mol^{-1}), which varies with the coverage and the form of the sample (evaporated film or powder) [13].

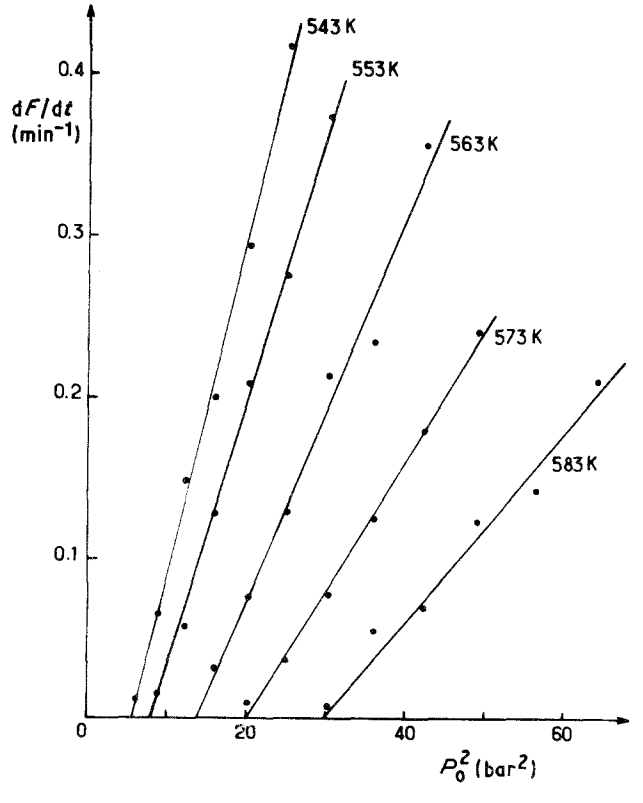

Figure 11 Dependence of the hydriding rate on the square of hydrogen pressure in the range of reacted fraction $\sim 0.05 < F \leqslant 0.25$.

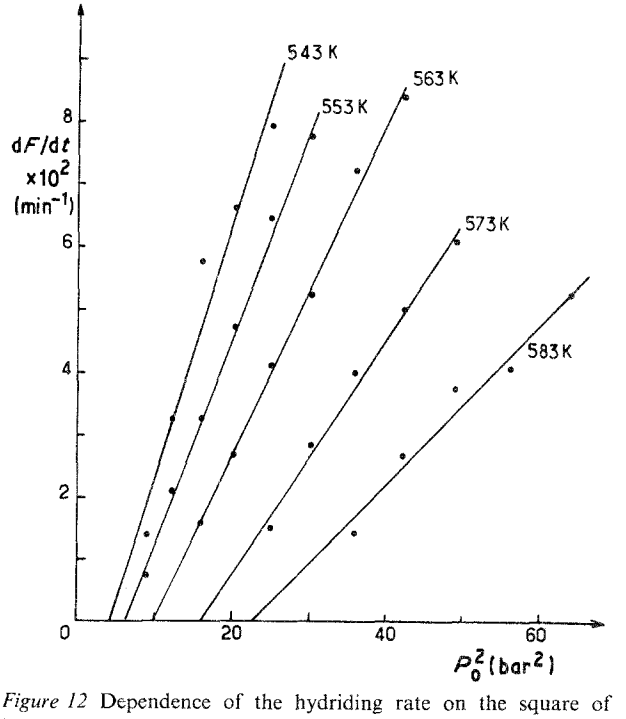

Figure 12 Dependence of the hydriding rate on the square of hydrogen pressure in the range of reacted fraction $0.60 < F \leqslant 0.70$.

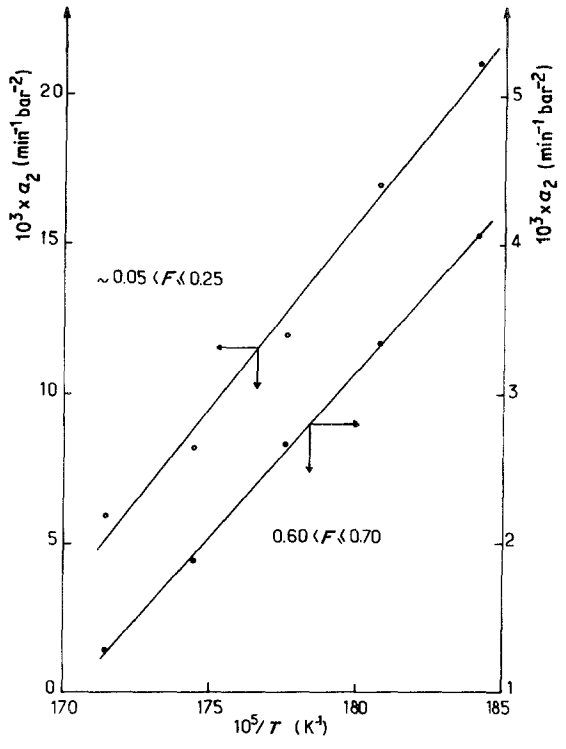

Figure 13 Plot of a_2 against T^{-1} for the forced-flow control.

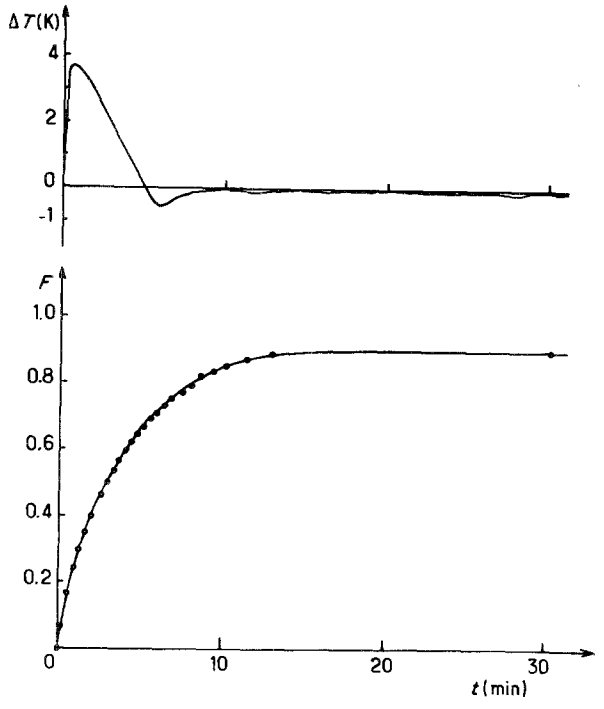

Figure 14 Variation of temperature along with hydriding reaction at 573 K under 7 bar H_2 (0.7 MPa).

This heat of formation of Mg_2Ni hydride and that of hydrogen chemisorption is the cause of the increase in temperature in the course of the hydriding reaction. In order to maintain isothermal conditions, as we cannot change the thermal conductivity of the sample, we can control the hydrogen absorption rate and thus the heat generation rate by reducing the amount of sample and/or by working under a lower driving force ($P_0 - P_{eq}$) and/or with a system having a large heat capacity [17].

The hydriding kinetics of the (Mg_2Ni + 2.7 wt % Ni)–H_2 system has been investigated in a parallel work [5]. The rate-controlling step for hydriding was analysed to be the dissociative chemisorption of hydrogen, involving also heat transfer control. In the (Mg_2Ni + 2.7 wt % Ni) sample more MgO was observed by X-ray diffraction than in the Mg_2Ni sample used in this work, due to another method of sample preparation. Under a pressure of 7 bar H_2 (0.7 MPa) at 573 K the (Mg_2Ni + 2.7 wt % Ni) of particle size smaller than 200 μm was activated only after seven hydrogen absorption–desorption cycles, while the Mg_2Ni used in this work, in which the particle size of the starting material was smaller than 63 μm, demanded 13 cycles for activation. The excess of nickel and MgO can be considered as making the material more brittle, causing many paths for the forced flow. This may explain why the rate-controlling step in (Mg_2Ni + 2.7 wt % Ni) hydriding is changed into dissociative chemisorption of hydrogen.

7. Conclusions

The hydriding reaction of Mg_2Ni progresses with the nucleation and growth mechanism. The rate-controlling step in the hydriding reaction of Mg_2Ni is the forced flow of hydrogen molecules through pores, interparticle channels or cracks, involving heat transfer control.

References

1. H. M. LUTZ and O. DE POUS, Proceedings of the 2nd International Congress on Hydrogen in Metals Paris, June 1977 (Pergamon Press, Oxford, 1977) p. 1F5.
2. K. NOMURA, E. AKIBA and S. ONO, *Int. J. Hydrogen Energy* **6** (3) (1981) 295.
3. E. AKIBA, K. NOMURA, S. ONO and S. SUDA, *ibid.* 7 (10) (1982) 787.
4. F. STUCKI, *ibid.* **8** (1) (1983) 49.
5. M. Y. SONG, M. PEZAT, B. DARRIET and P. HAGENMULLER, *J. Solid State Chem.* **56** (1985) 191.
6. W. B. PEARSON (editor), "A Handbook of Lattice Spacings and Structure of Metals and Alloys", Vol. 2 (Pergamon Press, New York, 1967).
7. M. Y. SONG, M. PEZAT, B. DARRIET and P. HAGENMULLER, *J. Mater. Sci.* **20** (1985) 2958.
8. A. SEILER, L. SCHLAPBACH, TH. VON WALDKIRCH, D. SHALTIEL and F. STUCKI, *J. Less-Common Metals* **73**, (1980) 193.
9. L. SCHLAPBACH, A. SEILER, F. STUCKI and H. C. SIEGMANN, *ibid.* **73**, (1980) 145.
10. T. B. FLANAGAN, Proceedings of International Symposium on Hydrides for Energy Storage, Geilo, August 1977 (Pergamon Press, Oxford, 1978) p. 135.
11. C. N. PARK, PhD thesis, Korean Advanced Institute of Science and Technology, 1982.
12. J. M. THOMAS and W. J. THOMAS, "Introduction to the Principles of Heterogeneous Catalysis" (Academic Press, London, 1967) p. 34.
13. G. C. BOND, "Catalysis by Metals" (Academic Press, London, 1962) p. 105.
14. KEITH J. LAIDLER, "Chemical Kinetics" (McGraw-Hill, New York, 1965) p. 260.
15. J. SZEKELY, J. W. EVANS and H. Y. SOHN, "Gas–Solid Reactions" (Academic Press, London, 1976) p. 39.
16. J. W. CHRISTIAN, "The Theory of Transformations in Metals and Alloys" (Pergamon Press, Oxford, 1965).
17. P. S. RUDMAN, *J. Less-Common Metals* **89** (1983) 93.

Received 24 July 1984
and accepted 28 February 1985